Damage Identification of Beams Using a Continuously Scanning Laser Doppler Vibrometer System

Da-Ming Chen
Department of Mechanical Engineering,
University of Maryland, Baltimore County,
1000 Hilltop Circle,
Baltimore, MD 21250
e-mail: damingc1@umbc.edu

Y. F. Xu
Department of Mechanical Engineering,
University of Maryland, Baltimore County,
1000 Hilltop Circle,
Baltimore, MD 21250
e-mail: yxu2@umbc.edu

W. D. Zhu[1]
Professor
Fellow ASME
Division of Dynamics and Control,
School of Astronautics,
Harbin Institute of Technology,
P.O. Box 137,
Harbin 150001, China;
Department of Mechanical Engineering,
University of Maryland, Baltimore County,
1000 Hilltop Circle,
Baltimore, MD 21250
e-mail: wzhu@umbc.edu

A continuously scanning laser Doppler vibrometer (CSLDV) system is capable of rapidly obtaining spatially dense operating deflection shapes (ODSs) by continuously sweeping a laser spot from the system over a structure surface. This paper presents a new damage identification methodology for beams that uses their ODSs under sinusoidal excitation obtained by a CSLDV system, where baseline information of associated undamaged beams is not needed. A curvature damage index (CDI) is proposed to identify damage near a region with high values of the CDI at an excitation frequency. The CDI uses the difference between curvatures of ODSs (CODSs) associated with ODSs that are obtained by two different CSLDV measurement methods, i.e., demodulation and polynomial methods; the former provides rapid and spatially dense ODSs of beams, and the latter provides ODSs that can be considered as those of associated undamaged beams. Phase variables are introduced to the two methods for damage identification purposes. Effects of the order in the polynomial method on qualities of ODSs and CODSs are investigated. A convergence index and a criterion are proposed to determine a proper order in the polynomial method. Effects of scan and sampling frequencies of a CSLDV system on qualities of ODSs and CODSs from the two measurement methods are investigated. The proposed damage identification methodology was experimentally validated on a beam with damage in the form of machined thickness reduction. The damage and its region were successfully identified in neighborhoods of prominent peaks of CDIs at different excitation frequencies. [DOI: 10.1115/1.4033639]

Keywords: continuously scanning laser Doppler vibrometer system, structural damage identification, demodulation method, polynomial method, curvature damage index

1 Introduction

Vibration-based damage detection has become a major research topic of structural dynamics in the past few decades. Since modal characteristics of a structure, i.e., natural frequencies, mode shapes, and modal damping ratios, are directly related to physical properties of the structure, such as mass, stiffness, and damping, measured modal characteristics can be processed to detect, locate, and characterize damage in the structure [1]. Methods that use changes of natural frequencies due to existence of damage have been investigated by many researchers. Some methods require minimum amounts of vibration measurements and can yield accurate estimation of positions and extent of damage, since natural frequencies are global characteristics of a structure and relatively easy to measure [2–5]. However, natural frequencies do not directly provide spatial information of structural changes due to damage, and accurate and physics-based models are needed to apply the methods, which can be difficult to construct in practice. Unlike natural frequencies, mode shapes directly provide spatial information of structural changes due to damage. Curvature mode shapes can be more sensitive to small damage than mode shapes and are often used to identify damage [6]. Comparing a curvature mode shape of a damaged beam with that of an undamaged beam, one can see that there is a global trend in the curvature mode shape of the damaged beam, which is similar to that of the undamaged one, and local abrupt abnormalities due to damage need to be isolated from the trend in order to identify the damage. Pandey et al. [6] showed that differences between curvature mode shapes of damaged and undamaged beams mainly exist in damage regions and increase as damage sizes increase. Ratcliffe [7] proposed a gapped smoothing method to identify damage in beams by inspecting smoothnesses of CODSs without using CODSs of undamaged beams. In the gapped smoothing method, the global trend of a curvature mode shape or CODS at a measurement point is eliminated using a gapped cubic polynomial that fits the curvature mode shape or CODS of its neighboring measurement points. However, the technique can be computationally inefficient for a large-sized dense measurement grid. Yoon et al. [8] combined the gapped smoothing method and a global fitting method to identify damage in beams, where generic mode shapes were used to fit measured mode shapes of damaged beams. However, accurate models are required to yield generic mode shapes, which can be unavailable in practice. Xu et al. [9] proposed a curvature mode-shape-based method to identify embedded horizontal cracks in beams, where global trends of curvature mode shapes were eliminated using curvature mode shapes from polynomials with properly determined orders that fit mode shapes of damaged beams. Xu et al. [10] proposed a noise-robust damage identification method for bars that used multiscale slope vibration shapes, which were calculated by applying a wavelet transform to slopes of longitudinal vibration shapes.

A laser Doppler vibrometer is a noncontact measurement instrument that can measure the surface velocity of a vibrating structure along the laser line-of-sight direction, using the Doppler shift between the incident light and the scattered light that returns to the instrument [11]. It has distinct advantages of measuring lightweight structures without having to attach a transducer that

[1]Corresponding author.

Contributed by the Technical Committee on Vibration and Sound of ASME for publication in the Journal of Vibration and Acoustics. Manuscript received October 6, 2015; final manuscript received May 3, 2016; published online June 17, 2016. Assoc. Editor: Patrick S. Keogh.

can locally stiffen or mass load the structures. A laser beam emitted from a laser Doppler vibrometer can be directed to any visible position on a structure by installing a scanner that consists of a pair of orthogonal scan mirrors in front of the laser Doppler vibrometer, and the whole system is called a scanning laser Doppler vibrometer system. This technique has greatly increased the spatial resolution of field measurement since the laser spot on the structure, resulting from the laser beam, can stay at one point long enough to acquire sufficient vibration data of that point and then move to the next one by controlling rotation angles of the scan mirrors.

The point-by-point measurement method using a scanning laser Doppler vibrometer system usually takes a long acquisition time in order to get a full-field measurement of a structure, especially when the measurement grid is large and dense. In the early 1990s, Sriram et al. [12,13] proposed a new scanning laser Doppler vibrometer measurement method where the laser spot was continuously swept over a surface of a structure under sinusoidal excitation; they also built a prototype of a CSLDV system. Since the laser spot continuously moves, the CSLDV velocity output is modulated by an ODS and can be processed in the frequency domain to directly obtain the ODS in the form of a Chebyshev series. Later, Stanbridge and Ewins [14,15] developed two CSLDV measurement methods to obtain ODSs of a structure under sinusoidal excitation, and the methods can be applied to different scan patterns, such as line scans, circular scans, and area scans. One measurement method is the demodulation method, where the CSLDV output is multiplied by sinusoidal signals at the excitation frequency and a low-pass filter is applied to obtain an ODS. The other one is the polynomial method, where an ODS is represented by a polynomial and its coefficients are obtained by processing the discrete Fourier transform of the CSLDV output. These two methods were also applied to structures under impact [16] and multisine [17] excitation. Allen and Sracic [18] proposed a "lifting" method to treat the CSLDV output of a structure as the free response of a linear time-periodic system and decompose it into a set of frequency response functions, from which mode shapes and modal damping ratios of the structure can be obtained using conventional curve fitting methods. This method was extended to output-only modal analysis to identify modal characteristics of a structure under unmeasurable broadband random excitation [19]. Yang and Allen [20] used a harmonic transfer function to process the CSLDV output of a downhill ski and obtain translational and rotational velocities with circular scans. Khan et al. [21] applied the demodulation method to measure ODSs of various structures with surface cracks. Short scan lines were assigned on cracked surfaces to intersect with the cracks, and discontinuities could be observed in the ODSs. However, discontinuities in ODSs may not be obvious when a scan line is on an intact surface with cracks existing on the opposite one.

This paper presents a new methodology to identify damage in beams that can be slender or thick using their ODSs under sinusoidal excitation obtained by a CSLDV system. The methodology does not require any baseline information of associated undamaged beams if the beams are geometrically smooth and made of materials that have no stiffness discontinuities. A CDI that uses the difference between CODSs associated with ODSs obtained by the demodulation and polynomial methods is proposed. Phase variables are introduced to the two methods, which control amplitudes of in-phase and quadrature components of measured ODSs, for damage identification purposes. Effects of the order in the polynomial method and scan and sampling frequencies of the CSLDV system on qualities of ODSs and CODSs are investigated. A new convergence index and a criterion are proposed to determine a proper order in the polynomial method for an ODS at an excitation frequency. An experimental investigation on a beam with damage in the form of machined thickness reduction was conducted. The damage and its region were successfully identified in neighborhoods of prominent peaks of CDIs at different excitation frequencies.

The remaining part of the paper is outlined as follows. The damage identification method using CODSs is presented in Sec. 2.1; the demodulation and polynomial methods for a CSLDV system are provided in Secs. 2.2.1 and 2.2.2, respectively. Effects of scan and sampling frequencies of a CSLDV system on qualities of measured ODSs and CODSs are investigated in Secs. 3.1 and 3.2, respectively; experimental damage identification results associated with different excitation frequencies are presented in Secs. 3.3 and 3.4. Conclusion of the work is presented in Sec. 4.

2 Methodology

2.1 Damage Identification Using CODSs. Effects of damage on an ODS of a beam in Fig. 1(*a*) can be manifested in its curvature, i.e., CODS, as shown in Fig. 1(*b*), which appear to be abrupt local abnormalities in the neighborhood of the damage. Note that white noise with a signal-to-noise ratio (SNR) of 90 is added to ODSs of damaged and undamaged beams in Fig. 1(*a*) to simulate measurement noise. A CODS can be calculated using a finite difference scheme

$$y''(x) = \frac{y(x-h) - 2y(x) + y(x+h)}{h^2} \tag{1}$$

where $y(x)$ is an ODS and h is the distance between the point x and either end of a derivative interval; h determines the resolution of the resulting curvature [9]. Adverse effects of measurement noise on calculation of a CODS can be alleviated by increasing the value of h, and a suitable value of h can be obtained by increasing it from a small one until a CODS with a low noise level is observed. Identification of the damage can be achieved by quantifying the effects of the damage on the CODS using a CDI, which can be expressed as

$$\phi(x) = \left[y_d''(x) - y_u''(x)\right]^2 \tag{2}$$

where $y_d''(x)$ and $y_u''(x)$ denote CODSs associated with an ODS of the damaged beam $y_d(x)$ and that of the associated undamaged one $y_u(x)$, respectively. The CDI in Eq. (2) is shown in Fig. 1(*c*), and the damage can be clearly identified near the region of high values of the CDI, which appears to be a prominent peak. When the ODS of the undamaged beam is not available, one can approximate it using a polynomial with a proper order that fits the ODS of the damaged beam. This technique was first proposed to identify embedded horizontal cracks in beams [9]. The ODS from a polynomial with an order of five that fits the ODS of the damaged beam and its CODS are shown in Figs. 1(*a*) and 1(*b*), respectively. It can be seen that the ODS from the polynomial fit is almost identical to that of the undamaged beam and the CODS from the polynomial fit well approximates that of the undamaged one except near boundaries of the beam. By comparing the CODS of the damaged beam with that from the polynomial fit, one can clearly identify the effects of the damage on a CDI, which is modified from that in Eq. (2) as

$$\psi(x) = \left[y_d''(x) - y_p''(x)\right]^2 \tag{3}$$

where $y_p''(x)$ denotes the CODS associated with the ODS from a polynomial fit $y_p(x)$. The CDI in Eq. (3) is shown in Fig. 1(*d*), and the damage can also be clearly identified in the neighborhood of a prominent peak in the CDI. The technique of approximating an ODS of an undamaged beam hinges on the order of the polynomial fit, and coefficients of the polynomial are determined by solving a least-squares problem. One needs to progressively try polynomials of different orders to find an optimal one for damage identification, which can be computationally inefficient especially for a large and dense measurement grid.

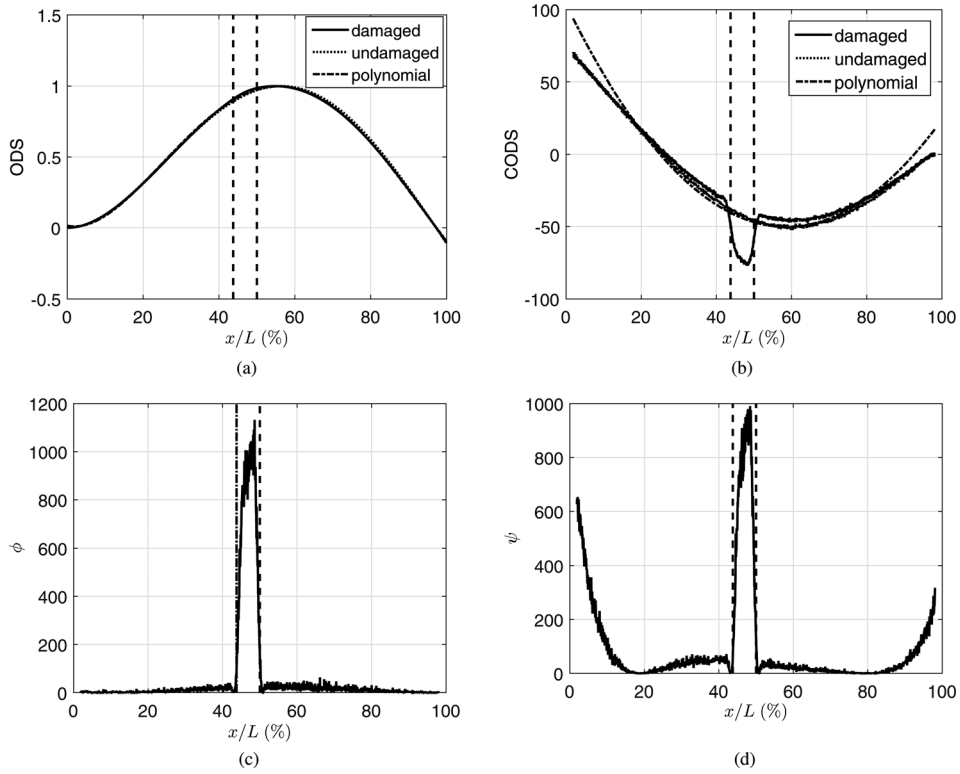

Fig. 1 (*a*) ODS of a beam with damage in the form of thickness reduction (damaged), that of an undamaged beam (undamaged) and that from a polynomial fit (polynomial); (*b*) CODSs associated with the ODSs in (*a*); (*c*) the CDI using the difference between the CODSs of the damaged and undamaged beams; and (*d*) the CDI using the difference between the CODS of the damaged beam and that from the polynomial fit. Locations of damage ends are indicated by two vertical dashed lines.

2.2 CSLDV System. In a CSLDV system, a laser spot is continuously swept over a vibrating structure surface by controlling its pair of orthogonal scan mirrors, called X and Y mirrors, which are connected to two independent stepper motors. Input signals to the stepper motors directly control rotation angles of the mirrors and create different scan patterns of the laser spot. Straight line scans are used in this work to obtain ODSs of a beam along its length by giving a triangular or sinusoidal input signal to the X mirror and a constant signal to the Y mirror. If a triangular signal is given to the X mirror, the amplitude of the rotation speed of the mirror is constant. It can be assumed that the resultant velocity of the laser spot on the beam is constant along the scan line when the rotation angle is sufficiently small. Likewise, if a sinusoidal signal is given to the X mirror, the resultant velocity of the laser spot on the beam can be assumed to be sinusoidal along the scan line. To obtain the ODS of a beam under sinusoidal excitation, the demodulation and polynomial methods are applied to the CSLDV output when triangular and sinusoidal signals are given to the X mirror, respectively. The CSLDV system developed in this work consists of a Cambridge 6240H scanner, a Polytec OFV-353 single-point laser vibrometer, and a dSPACE DS1103 controller board that controls the X and Y mirrors of the scanner, as shown in Fig. 2.

An experiment was set up to measure ODSs of a damaged aluminum beam using the CSLDV system, and dimensions of the beam are shown in Fig. 3(*a*). There was a region of machined thickness reduction on one side of the beam along its length, as shown in Fig. 3(*b*); the damage was selected in this form in order to show that its region can be accurately identified by the proposed methodology. The thickness reduction is about 20% of the thickness of the beam, and the location and length of the damage are shown in Fig. 3(*a*). A bench vice was used to clamp the left end of the beam to simulate a fixed boundary. A straight scan line was assigned on the intact side of the beam along its length. The scan line was nondimensionalized to range from 0% to 100%, where 0% and 100% represented left and right ends of the scan line shown in Fig. 3(*c*), respectively. The damage was located from 45.71% to 51.43% on the scan line. A strip of retroreflective

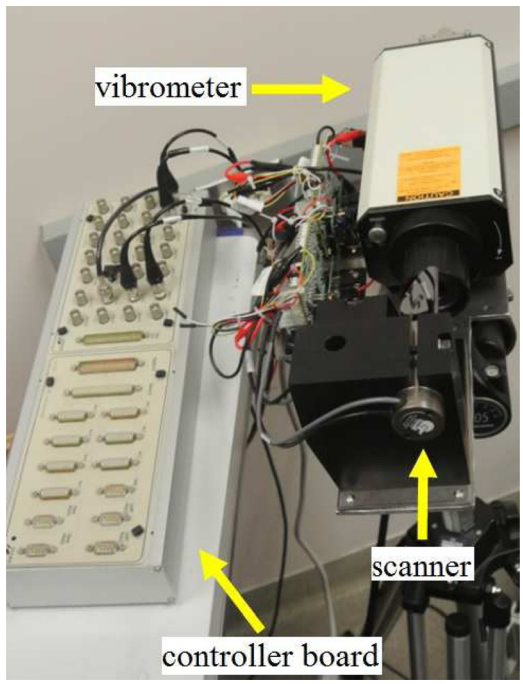

Fig. 2 The CSLDV system developed

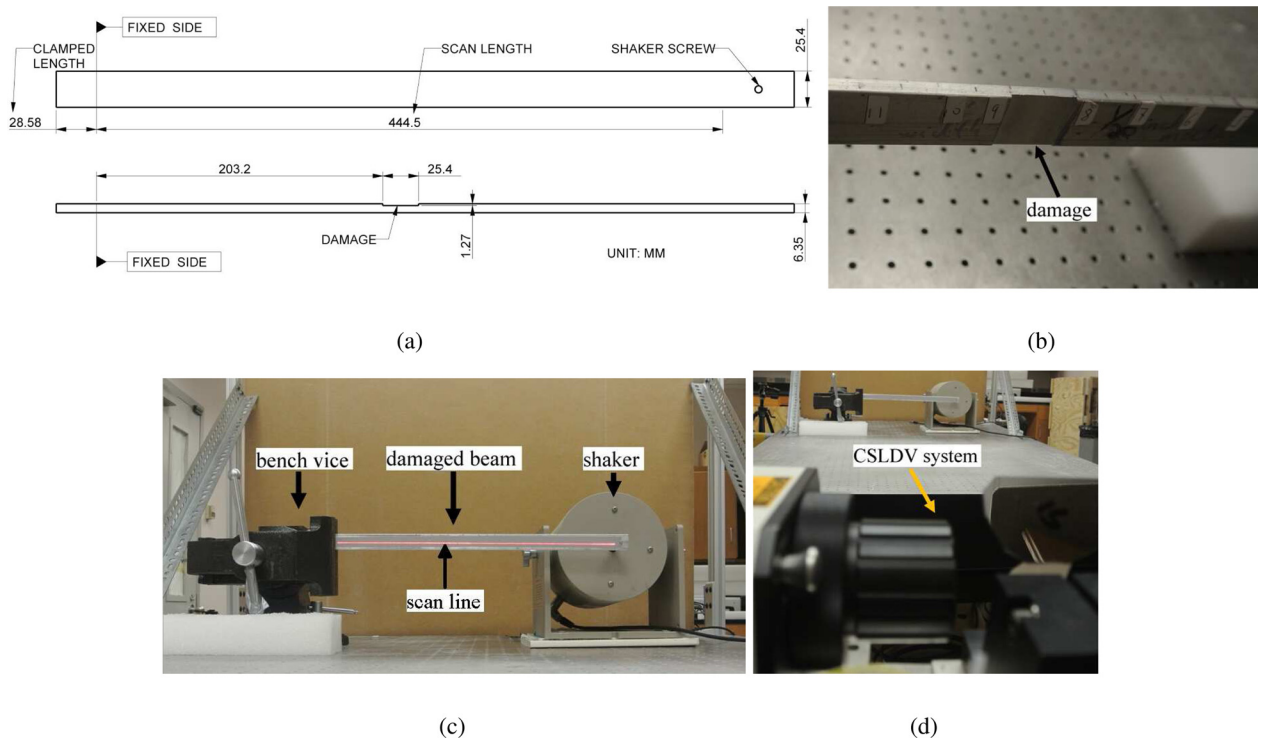

Fig. 3 (*a*) Dimensions of a damaged aluminum beam with a region of machined thickness reduction, (*b*) the region of machined thickness reduction, (*c*) the beam with its left end clamped by a bench vice and its right end connected to a shaker, and (*d*) the experimental setup for ODS measurements of the beam

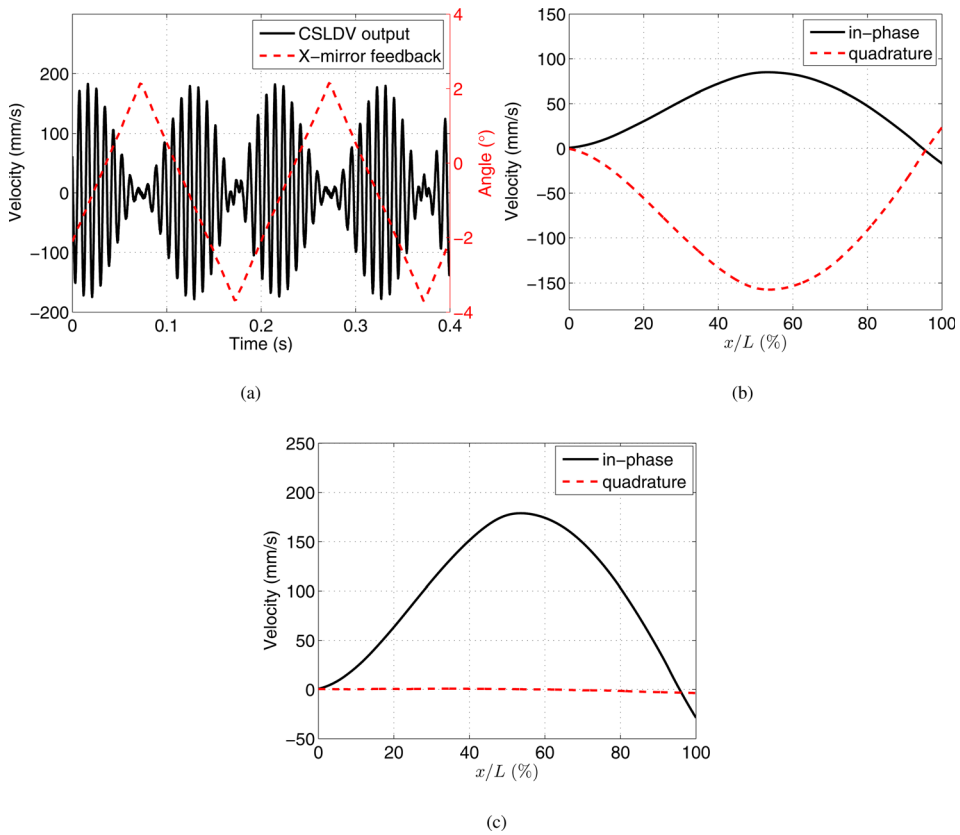

Fig. 4 (*a*) CSLDV velocity output of a beam at a sinusoidal excitation frequency of 111 Hz and the X-mirror feedback signal with a triangular input signal, (*b*) in-phase and quadrature ODS components from the demodulation method with $\theta = 0$ deg, and (*c*) in-phase and quadrature ODS components from the demodulation method with the optimal $\theta = 61.74$ deg

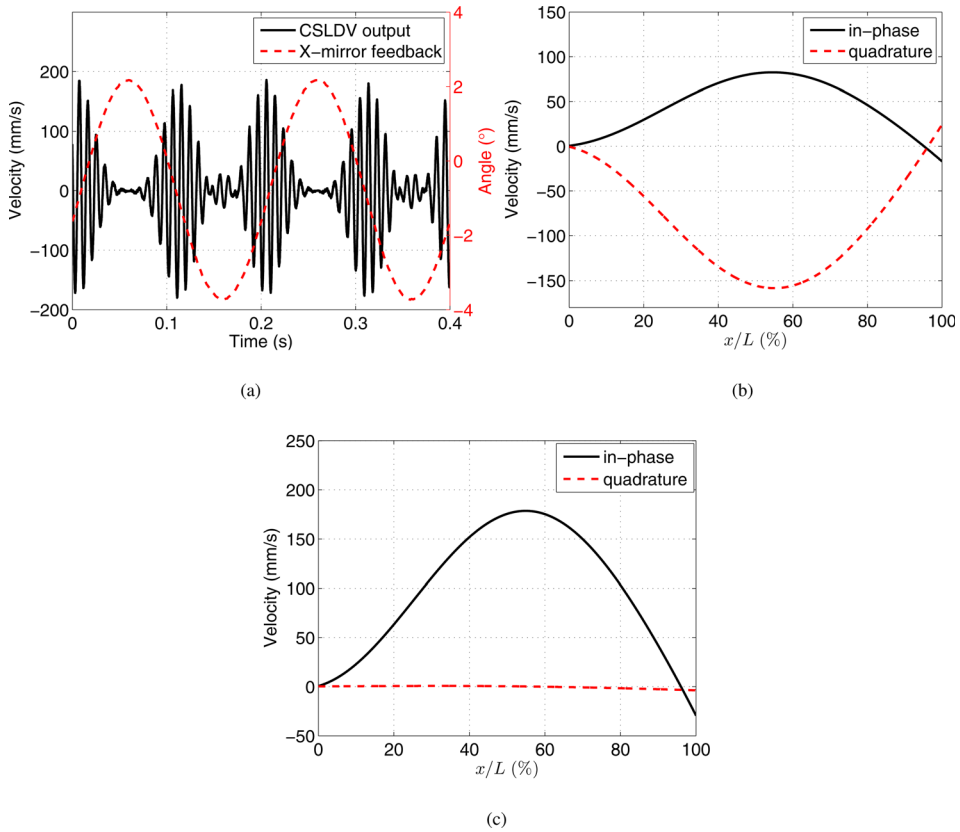

Fig. 5 (*a*) CSLDV velocity output of a beam at a sinusoidal excitation frequency of 111 Hz, and the X-mirror feedback signal with a sinusoidal input signal; (*b*) in-phase and quadrature ODS components from the polynomial method with $\gamma = 0$ deg; and (*c*) in-phase and quadrature ODS components from the polynomial method with the optimal $\gamma = 62.56$ deg

tape was attached on the intact side of the beam to enhance laser reflection that directly determined SNRs of the CSLDV velocity output. The experimental setup is shown in Figs. 3(*c*) and 3(*d*): a MB Dynamics MODAL-50 shaker was connected to the right end of the beam with a shaker screw, and the CSLDV system was used to measure velocity responses of the beam along the scan line. The sampling frequency of the CSLDV system was 32,000 Hz in this section.

2.2.1 Demodulation Method. The demodulation method proposed in Ref. [15] is modified here by introducing a phase variable θ for damage identification purposes. The steady-state response frequency of a linear time-invariant structure resulting from sinusoidal excitation is equal to the excitation frequency. When a CSLDV system measures the steady-state response of a structure under sinusoidal excitation and a triangular input signal is given to its X mirror, the velocity response of the structure measured by the system along a straight scan line can be expressed as

$$\begin{aligned} v_d(x,\,t) &= V_d(x)\cos(\omega t - \alpha - \theta) \\ &= V_{I,d}(x)\cos(\omega t) + V_{Q,d}(x)\sin(\omega t) \end{aligned} \tag{4}$$

where x is the location of the laser spot on the structure along the scan line, ω is the excitation frequency, $V_d(x)$ is the ODS of the structure along the scan line, α is the phase difference between the excitation and X-mirror feedback signal, and θ adjusts amplitudes of $V_{I,d}(x) = V_d(x)\cos(\alpha + \theta)$ and $V_{Q,d}(x) = V_d(x)\sin(\alpha + \theta)$, which are in-phase and quadrature ODS components, respectively. In order to obtain $V_{I,d}(x)$ and $V_{Q,d}(x)$ from the CSLDV output, $v_d(x,t)$ in Eq. (4) is multiplied by $\cos(\omega t)$ and $\sin(\omega t)$, which gives

$$\begin{aligned} &v_d(x,\,t)\cos\omega t \\ &\quad = V_{I,d}(x)\cos\omega t\cos\omega t + V_{Q,d}(x)\sin\omega t\cos\omega t \\ &\quad = \frac{1}{2}V_{I,d}(x) + \frac{1}{2}V_{I,d}(x)\cos 2\omega t + \frac{1}{2}V_{Q,d}(x)\sin 2\omega t \end{aligned} \tag{5}$$

$$\begin{aligned} &v_d(x,\,t)\sin\omega t \\ &\quad = V_{I,d}(x)\cos\omega t\sin\omega t + V_{Q,d}(x)\sin\omega t\sin\omega t \\ &\quad = \frac{1}{2}V_{Q,d}(x) + \frac{1}{2}V_{I,d}(x)\sin 2\omega t - \frac{1}{2}V_{Q,d}(x)\cos 2\omega t \end{aligned} \tag{6}$$

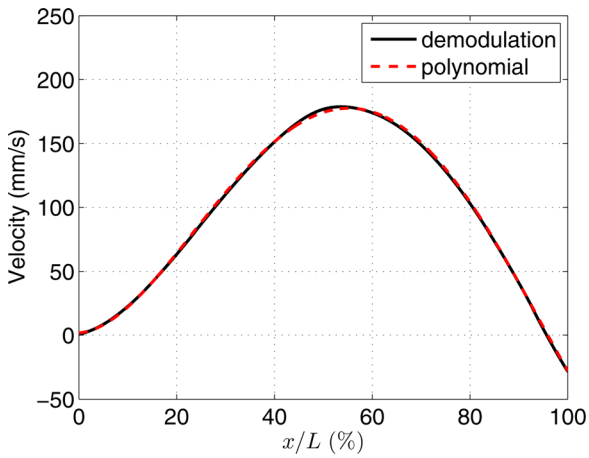

Fig. 6 Comparison between ODSs from the demodulation method and the polynomial method with $m = 5$

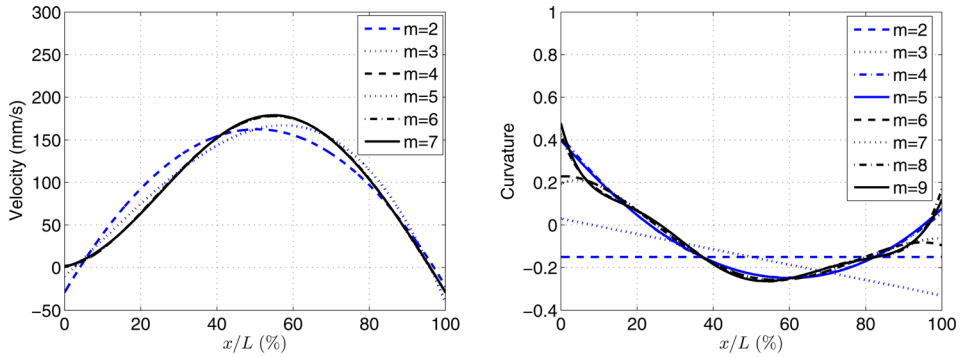

Fig. 7 (*a*) ODSs from the polynomial method with *m* ranging from two to seven and (*b*) CODSs from the polynomial method with *m* ranging from two to nine

respectively. Second and third terms on the third lines of Eqs. (5) and (6) can be eliminated by applying a low-pass filter to $v_d \cos \omega t$ and $v_d \sin \omega t$ to yield $(1/2)V_{I,d}(x)$ and $(1/2)V_{Q,d}(x)$, respectively. Further, $V_{I,d}(x)$ and $V_{Q,d}(x)$ can be obtained by multiplying corresponding filtered signals by two, which completes the demodulation method.

The CSLDV output of the beam in Fig. 3 under sinusoidal excitation by the shaker at an excitation frequency of 111 Hz and the X-mirror feedback signal are shown in Fig. 4(*a*). Note that a triangular signal was given to the X mirror and the scan frequency was 5 Hz. The X-mirror feedback signal was used to determine the location of the laser spot, based on which one can extract an end-to-end ODS of the beam under the excitation. In-phase and quadrature ODS components obtained by the demodulation method with $\theta = 0$ deg are shown in Fig. 4(*b*). Hereafter, the value of θ is optimized to be the one with which $V_{I,d}(x)$ and $V_{Q,d}(x)$ have their maximum and minimum amplitudes, respectively. In this case, the optimal value of θ is 61.74 deg and resulting in-phase and quadrature ODS components are shown in Fig. 4(*c*). The spatial resolution of an ODS obtained by the demodulation method is determined by sampling and scan frequencies. With the frequency settings in this case, the ODS is made up by $32,000/(5 \times 2) = 3200$ measurement points along the scan line from one end of the beam to the other. With a higher sampling frequency and a lower scan frequency, the spatial resolution of a resulting ODS from the demodulation method is higher.

2.2.2 Polynomial Method. The polynomial method proposed in Ref. [15] is modified here by introducing a phase variable γ for damage identification purposes. Note that γ differs from θ in the demodulation method in Sec. 2.2.1. In-phase and quadrature ODS components can be represented using polynomials along the scan line [15]. The scan line can be normalized using the "center and scale" technique [22] and expressed as

$$\hat{x}(t) = \frac{2x(t) - 2\bar{x}}{l} \tag{7}$$

where $\bar{x}$ is the position of the middle point of the scan line and l is its length; the domain of $\hat{x}$ is $[-1, 1]$. When a sinusoidal input signal is given to the X mirror, the instantaneous location of the laser spot on the normalized scan line can be expressed as

$$\hat{x}(t) = \cos(\Omega t + \beta) \tag{8}$$

where Ω is the scan frequency and β is the phase difference between the excitation and X-mirror feedback signal. The CSLDV output $v_p(\hat{x}, t)$ can be expressed as

$$v_p(\hat{x}, t) = V_p(\hat{x})\cos(\omega t - \gamma) = V_{I,p}(\hat{x})\cos(\omega t) + V_{Q,p}(\hat{x})\sin(\omega t) \tag{9}$$

where γ is a phase variable that adjusts amplitudes of $V_{I,p}(\hat{x}) = V_p(\hat{x})\cos\gamma$ and $V_{Q,p}(\hat{x}) = V_p(\hat{x})\sin\gamma$, which are in-phase and quadrature ODS components, respectively. The ODS components $V_{I,p}(\hat{x})$ and $V_{Q,p}(\hat{x})$ can be represented by polynomials; substituting Eq. (8) into the polynomials yields

$$V_{I,p}(\hat{x}) = \sum_{n=0}^{m} V_{In}\hat{x}^n = \sum_{n=0}^{m} V_{In}\cos^n(\Omega t + \beta) \tag{10}$$

$$V_{Q,p}(\hat{x}) = \sum_{n=0}^{m} V_{Qn}\hat{x}^n = \sum_{n=0}^{m} V_{Qn}\cos^n(\Omega t + \beta) \tag{11}$$

respectively, where V_{In} and V_{Qn} are coefficients of the polynomials, and m is their order. With substitution of Eqs. (10) and (11) into Eq. (9), $v_p(\hat{x}, t)$ can be expressed as

$$\begin{aligned} v_p(\hat{x}, t) &= \sum_{n=0}^{m} V_{In}\cos^n(\Omega t+\beta)\cos\omega t + \sum_{n=0}^{m} V_{Qn}\cos^n(\Omega t+\beta)\sin\omega t \\ &= \sum_{n=0}^{m} A_{In}\Big\{\cos\big[(\omega-n\Omega)t-n\beta\big] + \cos\big[(\omega+n\Omega)t+n\beta\big]\Big\} \\ &\quad + \sum_{n=0}^{m} A_{Qn}\Big\{\sin\big[(\omega-n\Omega)t-n\beta\big] + \sin\big[(\omega+n\Omega)t+n\beta\big]\Big\} \end{aligned} \tag{12}$$

where A_{In} and A_{Qn} are Fourier coefficients, which can be calculated by

$$\begin{aligned} A_{In} = \frac{1}{T}\Bigg\{ &\int_0^T v_p(\hat{x}, t)\cos\big[(\omega - n\Omega)t - n\beta\big]dt \\ &+ \int_0^T v_p(\hat{x}, t)\cos\big[(\omega + n\Omega)t + n\beta\big]dt\Bigg\} \end{aligned} \tag{13}$$

$$\begin{aligned} A_{Qn} = \frac{1}{T}\Bigg\{ &\int_0^T v_p(\hat{x}, t)\sin\big[(\omega - n\Omega)t - n\beta\big]dt \\ &+ \int_0^T v_p(\hat{x}, t)\sin\big[(\omega + n\Omega)t + n\beta\big]dt\Bigg\} \end{aligned} \tag{14}$$

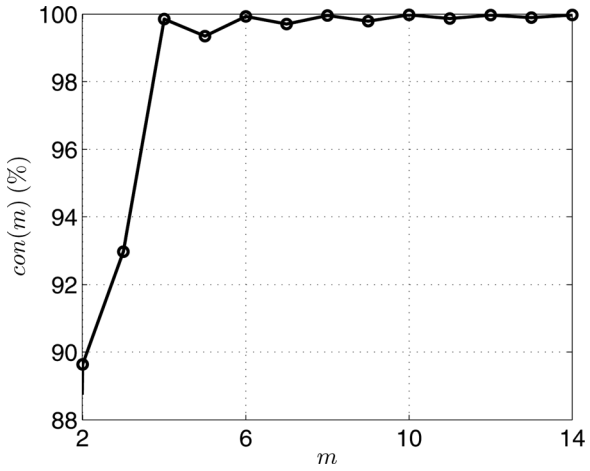

Fig. 8 Convergence index con(*m*) associated with ODSs from the polynomial method with *m* up to 14

and V_{In} and V_{Qn} can be calculated by [23]

$$\{\mathbf{V}_I\} = [\mathbf{T}_{m+1}]\{\mathbf{A}_I\} \tag{15}$$

$$\{\mathbf{V}_Q\} = [\mathbf{T}_{m+1}]\{\mathbf{A}_Q\} \tag{16}$$

respectively, where $\{\mathbf{V}_I\} = \{V_{I0}, \ldots, V_{Im}\}^{\mathrm{T}}$, $\{\mathbf{A}_I\} = \{A_{I0}, \ldots, A_{Im}\}^{\mathrm{T}}$, $\{\mathbf{V}_Q\} = \{V_{Q0}, \ldots, V_{Qm}\}^{\mathrm{T}}$, $\{\mathbf{A}_Q\} = \{A_{Q0}, \ldots, A_{Qm}\}^{\mathrm{T}}$, and $\mathbf{T}_{m+1}$ is an $(m+1)\times(m+1)$ transformation matrix, which is calculated in the Appendix. This completes the polynomial method.

The CSLDV output of the beam in Fig. 3 under sinusoidal excitation by the shaker at an excitation frequency of 111 Hz and the X-mirror feedback signal are shown in Fig. 5(*a*). Note that a sinusoidal signal was given to the X mirror and the scan frequency was 5 Hz. Figure 5(*b*) shows in-phase and quadrature ODS components obtained by the polynomial method with $\gamma = 0$ deg. Similar to the demodulation method, γ can be optimized so that $V_{I,p}(\hat{x})$ and $V_{Q,p}(\hat{x})$ have their maximum and minimum amplitudes, respectively. In this case, the optimal value of γ is 62.56 deg, and resulting $V_{I,p}(\hat{x})$ and $V_{Q,p}(\hat{x})$ are shown in Fig. 5(*c*). Since amplitudes of in-phase ODS components can be maximized and those of quadrature ODS components can be minimized in the demodulation and polynomial methods by optimizing θ and γ, respectively, one can use the in-phase ODS components with maximum amplitudes from the two methods at the same excitation frequency to represent the ODSs for damage identification that follows. In this paper hereafter, all ODSs are represented by their in-phase components with maximum amplitudes. The ODSs from the two methods are compared in Fig. 6, and it can be seen that they are almost identical. Note that optimal θ and γ do not have to be equal for maximizing amplitudes of in-phase ODS components since their values depend on phase differences between excitation and X-mirror feedback signals in the two methods.

Details of the demodulation and polynomial methods have been summarized above. An ODS from the demodulation method can be considered to be measured in a point-by-point manner. The main advantage of this method is that an accurate and spatially dense ODS can be rapidly obtained. Hence, local abrupt abnormalities caused by damage can be observed in an associated CODS with a high spatial resolution. The polynomial method assumes that in-phase and quadrature components of an ODS can be represented by polynomials. Similar to the CODS from a polynomial fit in Sec. 2.1, a CODS associated with an ODS from the polynomial method cannot capture local abrupt abnormalities caused by damage either, but it can be used to eliminate the global trend of a CODS from the demodulation method. It is proposed that a CDI based on CODSs from the two methods be used to identify damage, which can be expressed as

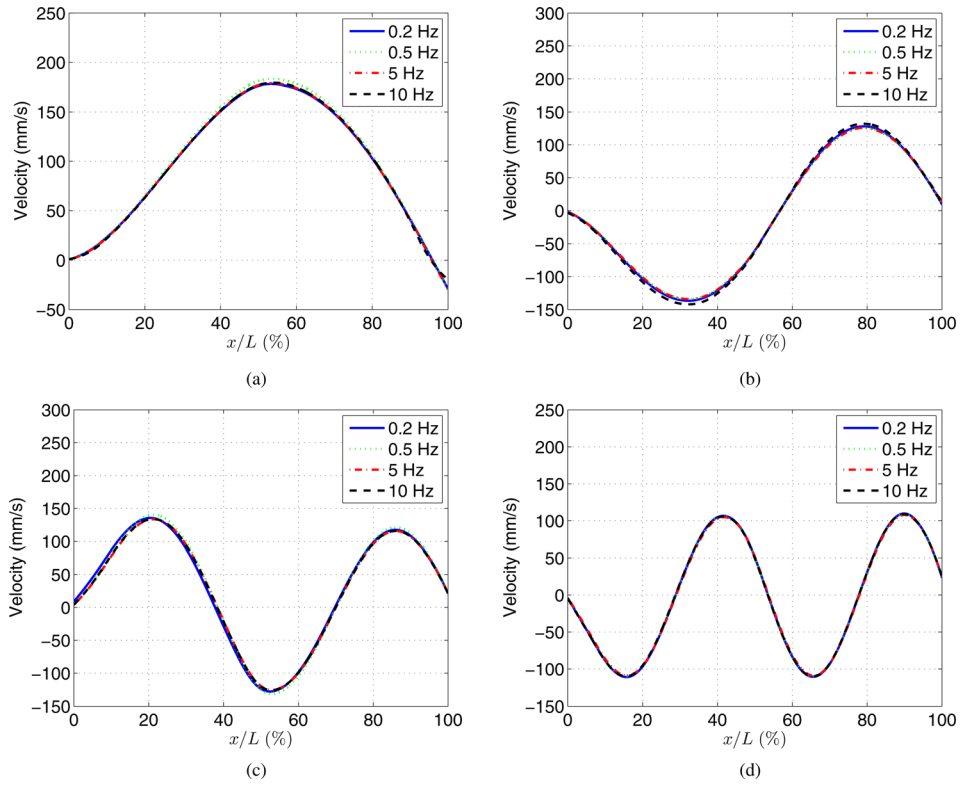

Fig. 9 ODSs of the damaged beam with different scan frequencies at excitation frequencies of (*a*) 111 Hz, (*b*) 335 Hz, (*c*) 688 Hz, and (*d*) 1193 Hz; all the ODSs were obtained by the demodulation method

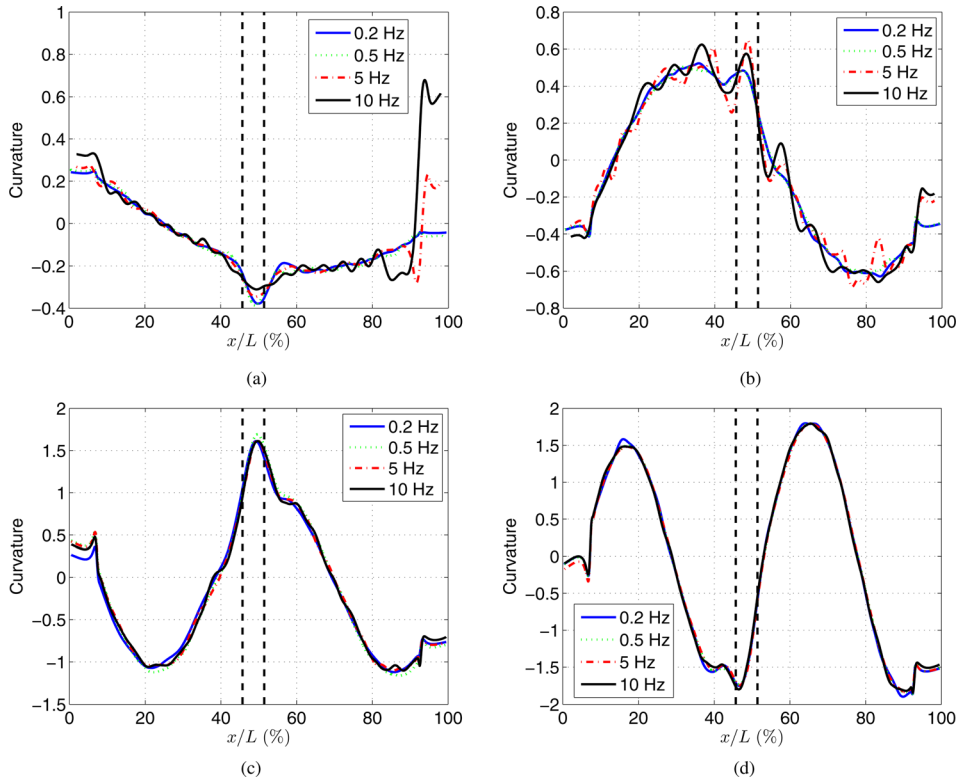

Fig. 10 CODSs of the damaged beam with different scan frequencies at excitation frequencies of (*a*) 111 Hz, (*b*) 335 Hz, (*c*) 688 Hz, and (*d*) 1193 Hz; all the ODSs associated with the CODSs were obtained by the demodulation method. Locations of damage ends are indicated by two vertical dashed lines.

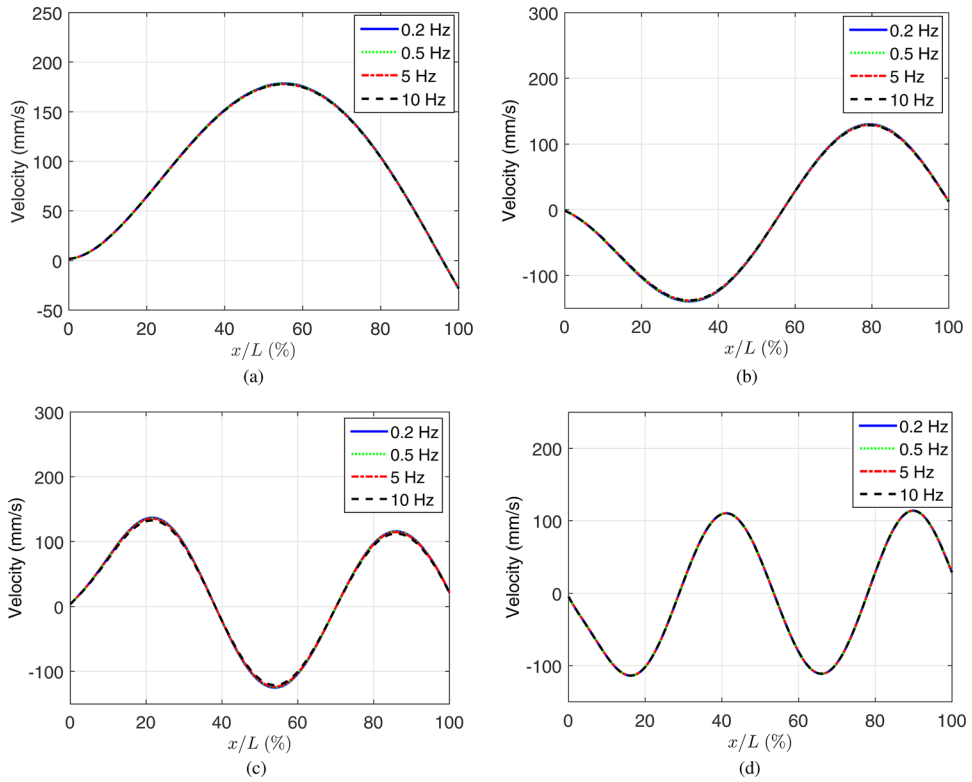

Fig. 11 (*a*) ODSs from the polynomial method with $m = 5$ with different scan frequencies at an excitation frequency of 111 Hz, (*b*) ODSs from the polynomial method with $m = 7$ with different scan frequencies at an excitation frequency of 335 Hz, (*c*) ODSs from the polynomial method with $m = 8$ with different scan frequencies at an excitation frequency of 688 Hz, and (*d*) ODSs from the polynomial method with $m = 9$ with different scan frequencies at an excitation frequency of 1193 Hz

$$\delta(x) = \left[V''_{I,d}(x) - V''_{I,p}(x)\right]^2 \tag{17}$$

where $V''_{I,d}(x)$ and $V''_{I,p}(x)$ are CODSs from the demodulation and polynomial methods, respectively. Damage can be identified near a region of high values of the CDI at an excitation frequency.

Validity of an ODS from the polynomial method is directly determined by m in Eqs. (10) and (11), but there has not been a guideline in determining a proper value of m possibly because an associated benchmark ODS does not exist in most cases. Hence, one has to determine m based on experience or a priori knowledge of the ODS. Figure 7(*a*) shows ODSs from the polynomial method with m ranging from two to seven; it can be observed that the ODSs converge, i.e., they do not significantly change, when $m \geq 4$. However, CODSs shown in Fig. 7(*b*) keep changing as m increases; waves can even be seen in the CODSs when $m \geq 8$, which are physically erroneous for the beam. To determine the proper value of m in the polynomial method for damage identification, a new convergence index is defined as

$$\text{con}(m) = \frac{\text{RMS}(\{\mathbf{V}_m\})}{\text{RMS}(\{\mathbf{V}_m\}) + \text{RMS}\left(\{\mathbf{V}_m\} - \{\mathbf{V}_{m+1}\}\right)} \times 100\% \tag{18}$$

where $\text{RMS}(\cdot)$ denotes the root mean square of a vector and $\{\mathbf{V}_m\}$ is the ODS vector from the polynomial method with the order m. If $\text{con}(m)$ is 100%, $\{\mathbf{V}_m\}$ is completely convergent and identical to $\{\mathbf{V}_{m+1}\}$; the higher $\text{con}(m)$, the more convergent $\{\mathbf{V}_m\}$ to $\{\mathbf{V}_{m+1}\}$. It is proposed in this work that the proper value of m be two plus the least value of m with which $\text{con}(m)$ is above 90%. Two is added here in order to preserve smoothness of the CODS from the polynomial method, since calculation of a curvature incurs second-order differentiation, which reduces the order of a polynomial by two. In this case, the proper value of m is five since $\text{con}(2) = 89.64\%$ and $\text{con}(3) = 92.97\%$, and $\text{con}(m)$ converges to 100% as m increases, as shown in Fig. 8.

3 Experimental Investigation

To experimentally investigate the proposed methodology, velocity responses of the beam in Fig. 3 under sinusoidal excitation by the shaker at different frequencies were measured by the CSLDV system with different scan and sampling frequencies. ODSs of the beam were obtained by the demodulation and polynomial methods, and damage identification results were analyzed to validate the proposed methodology.

An impact test was conducted on the beam in Fig. 3(*c*) to measure its first four natural frequencies; a PCB 086C03 impact hammer and the single-point laser Doppler vibrometer in Fig. 2 were used to excite the beam at an impact point and measure its response at a measurement point, receptively. Both the impact and measurement points on the beam were arbitrarily selected as long as they did not coincide with nodal points of its first four modes, since natural frequencies are global characteristics of the beam. The beam was sinusoidally excited by the shaker at different frequencies of 111 Hz, 335 Hz, 688 Hz, and 1193 Hz to investigate effects of scan and sampling frequencies of the CSLDV system on qualities of measured ODSs and CODSs; the excitation frequencies were obtained by rounding the first through fourth natural frequencies of the beam in the current experimental setup, respectively.

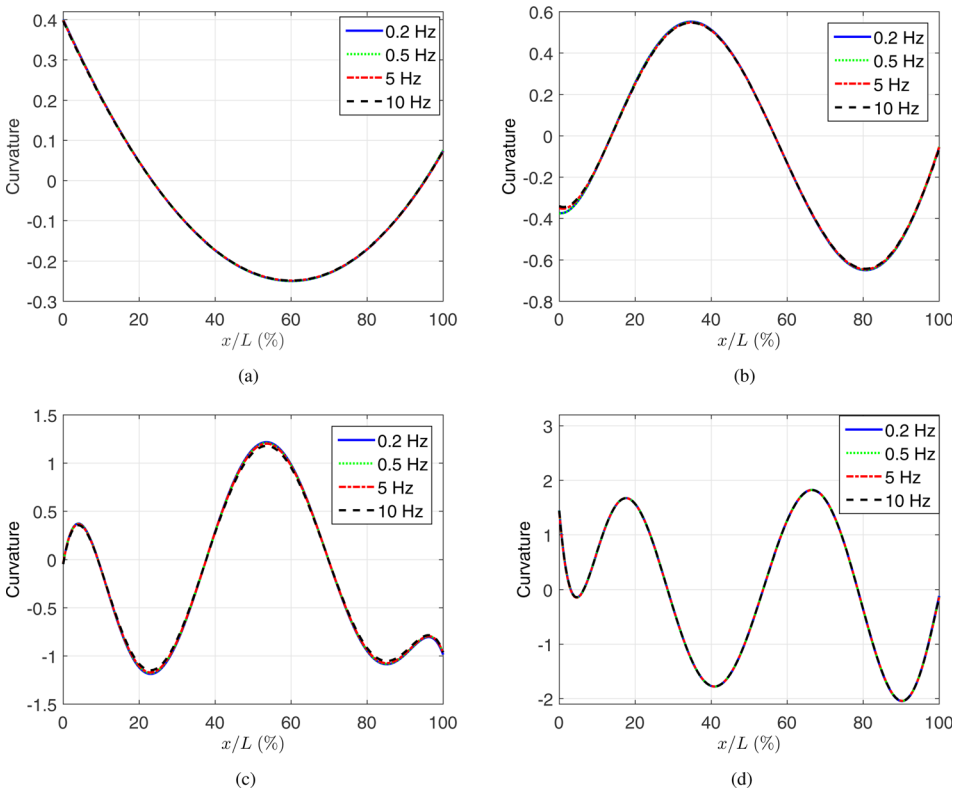

Fig. 12 (*a*) CODSs associated with the ODSs from the polynomial method with $m = 5$ with different scan frequencies at an excitation frequency of 111 Hz, (*b*) CODSs associated with the ODSs from the polynomial method with $m = 7$ with different scan frequencies at an excitation frequency of 335 Hz, (*c*) CODSs associated with the ODSs from the polynomial method with $m = 8$ with different scan frequencies at an excitation frequency of 688 Hz, and (*d*) CODSs associated with the ODSs from the polynomial method with $m = 9$ with different scan frequencies at an excitation frequency of 1193 Hz

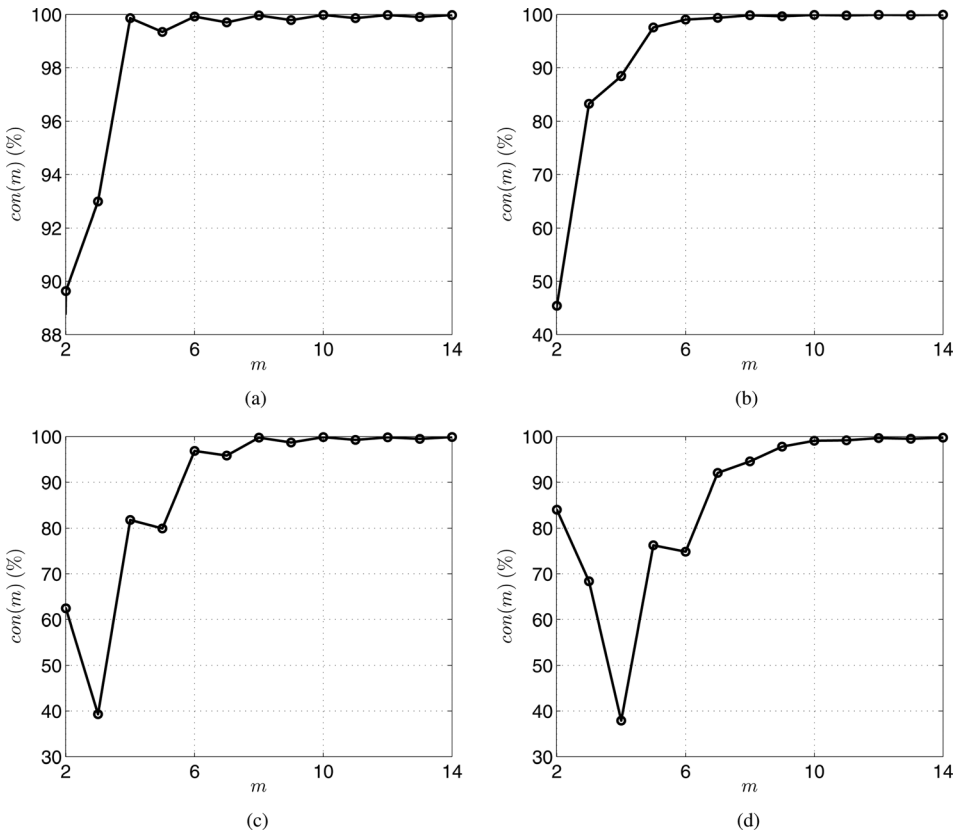

Fig. 13 Convergence indices con(*m*) associated with ODSs from the polynomial method with *m* up to 14 with a scan frequency of 0.2 Hz at excitation frequencies of (*a*) 111 Hz, (*b*) 335 Hz, (*c*) 688 Hz, and (*d*) 1193 Hz

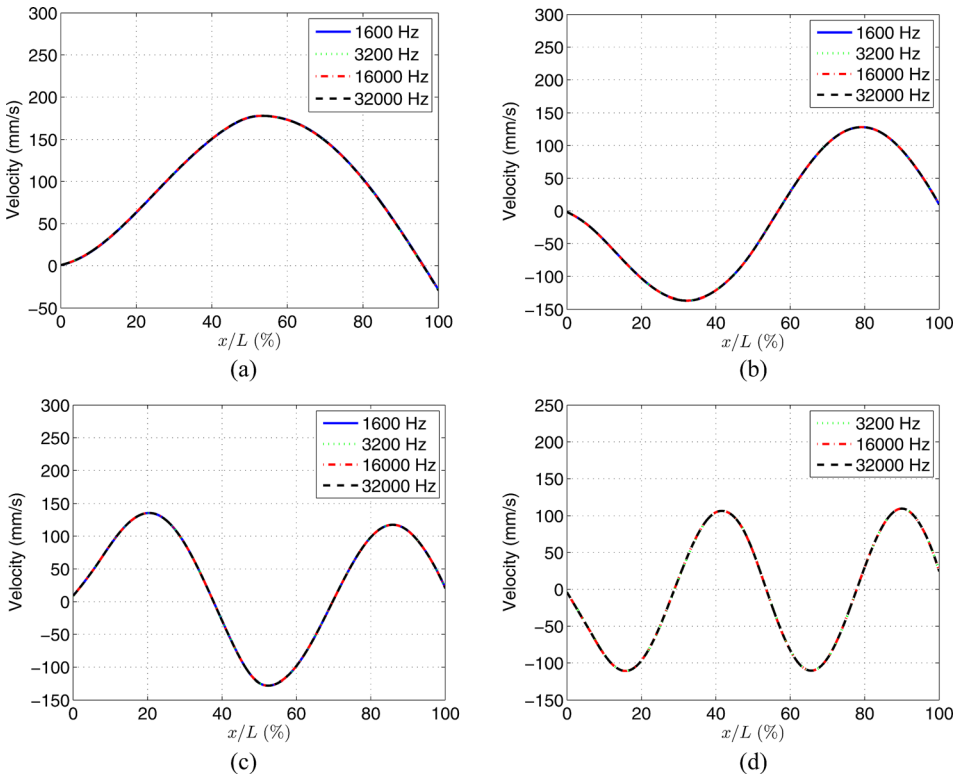

Fig. 14 ODSs of the damaged beam with different sampling frequencies at excitation frequencies of (*a*) 111 Hz, (*b*) 335 Hz, (*c*) 688 Hz, and (*d*) 1193 Hz; all the ODSs were obtained by the demodulation method

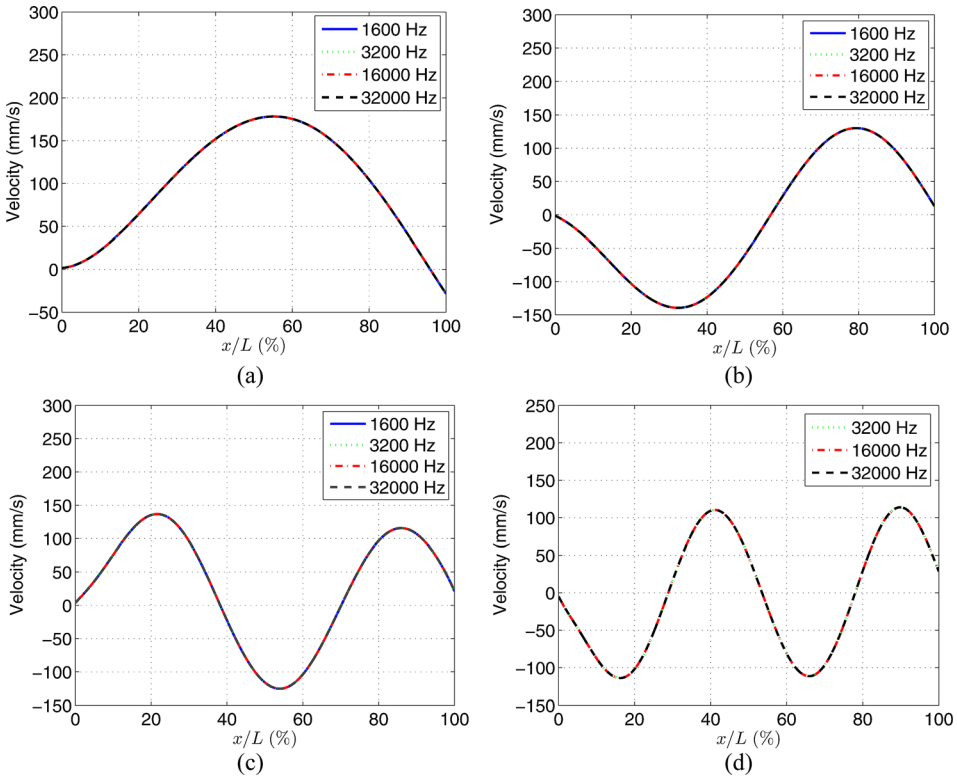

Fig. 15 ODSs of the damaged beam with different sampling frequencies at excitation frequencies of (*a*) 111 Hz, (*b*) 335 Hz, (*c*) 688 Hz, and (*d*) 1193 Hz; all the ODSs were obtained by the polynomial method

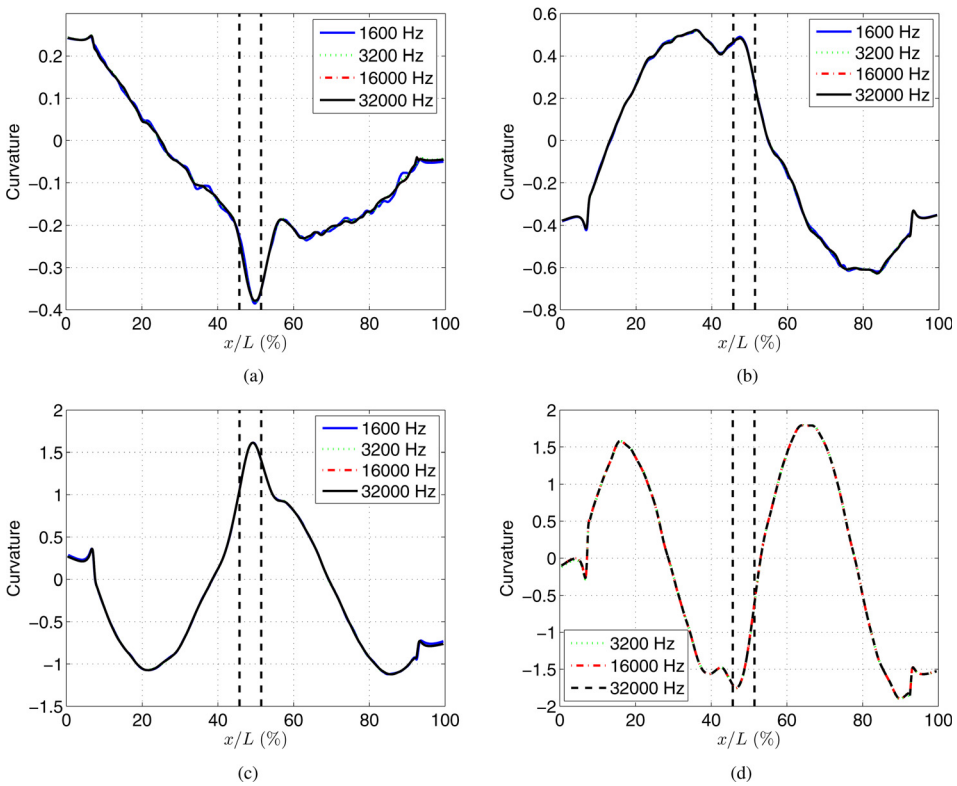

Fig. 16 CODSs of the damaged beam with different sampling frequencies at excitation frequencies of (*a*) 111 Hz, (*b*) 335 Hz, (*c*) 688 Hz, and (*d*) 1193 Hz; all the ODSs associated with the CODSs were obtained by the demodulation method. Locations of damage ends are indicated by two vertical dashed lines.

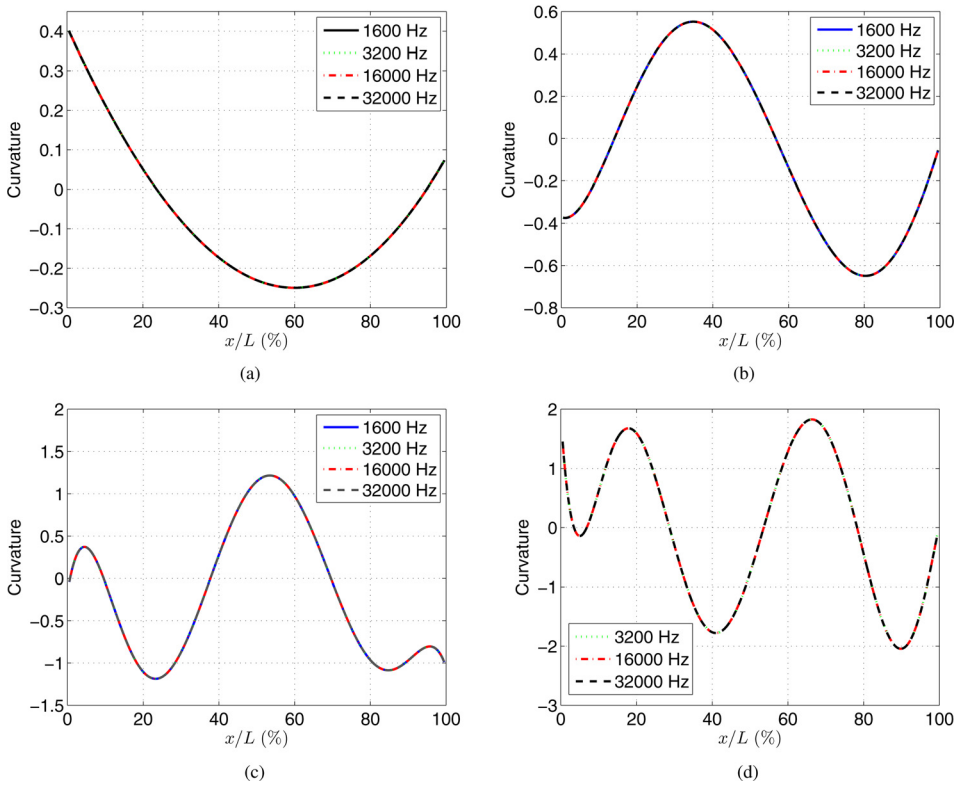

Fig. 17 CODSs of the damaged beam with different sampling frequencies at excitation frequencies of (*a*) 111 Hz, (*b*) 335 Hz, (*c*) 688 Hz, and (*d*) 1193 Hz; all the ODSs associated with the CODSs were obtained by the polynomial method

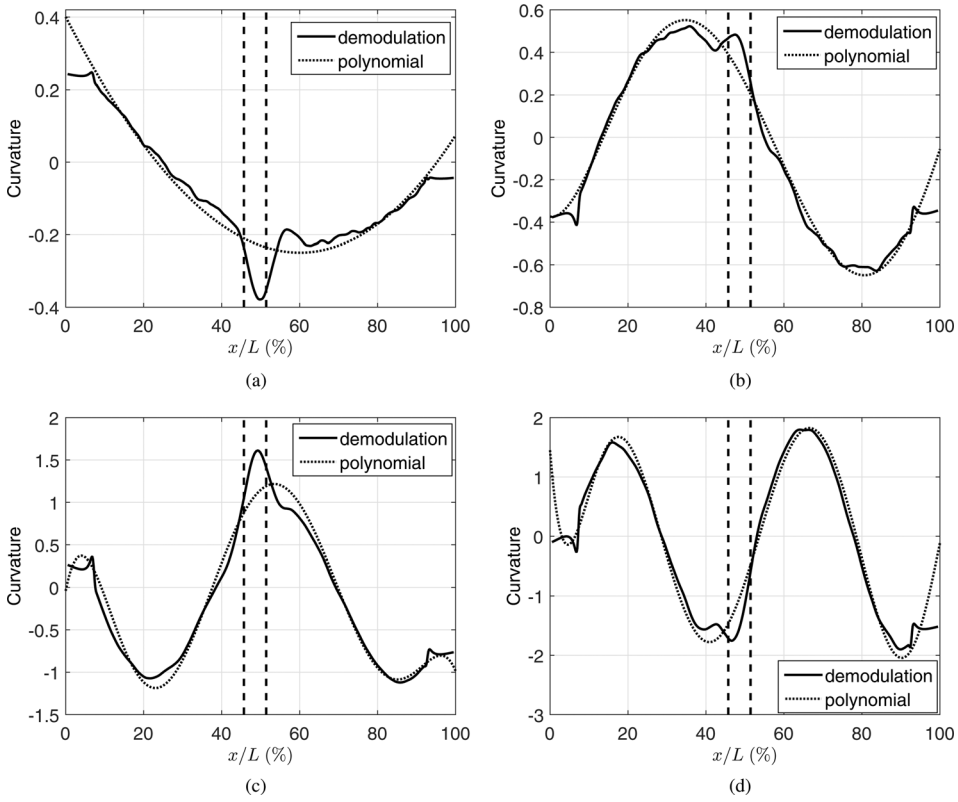

Fig. 18 Comparisons between CODSs from the demodulation and polynomial methods at excitation frequencies of (*a*) 111 Hz, (*b*) 335 Hz, (*c*) 688 Hz, and (*d*) 1193 Hz. Locations of damage ends are indicated by two vertical dashed lines.

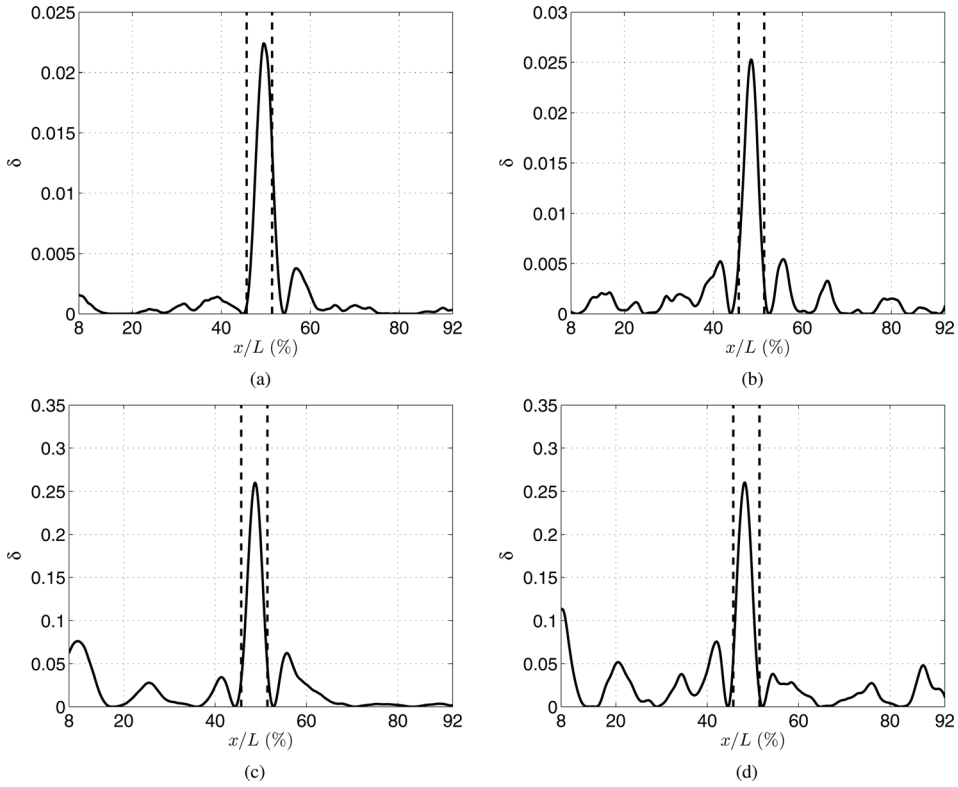

Fig. 19 CDIs at excitation frequencies of (*a*) 111 Hz, (*b*) 335 Hz, (*c*) 688 Hz, and (*d*) 1193 Hz. Locations of damage ends are indicated by two vertical dashed lines.

3.1 Effects of the Scan Frequency of the CSLDV System

3.1.1 ODSs and CODSs From the Demodulation Method. ODSs of the beam at the excitation frequencies were obtained by the demodulation method with different scan frequencies of 0.2 Hz, 0.5 Hz, 5 Hz, and 10 Hz and a sampling frequency of 32,000 Hz, as shown in Fig. 9. It could be observed that the ODSs at each excitation frequency, though measured with different scan frequencies, agreed well with one another. In the region of the damage, the ODSs were smooth since ODSs were not sensitive to the damage, and one could not identify it using the ODSs.

CODSs associated with the ODSs were calculated using Eq. (1) with h equal to 0.5% of the length of the scan line, as shown in Fig. 10. Note that measurement noise in the ODSs was reduced before calculation of the CODSs by applying a numerical smoothing method, which is local regression using weighted linear least squares and a second-order polynomial model; the method was performed using MATLAB. In the smoothing method, weighted quadratic least squares are calculated at each measurement point within an interval that consists of a certain number of its neighboring points, which was 15% of the total number of measurement points in this work. Local abrupt abnormalities in the form of a prominent peak could be seen in each CODS, which was caused by the damage, since the CODSs were sensitive to it. The effect of scan frequencies on qualities of CODSs could be seen by comparing the CODSs at each excitation frequency in Fig. 10. For the CODSs at the first two excitation frequencies, their qualities were better when a lower scan frequency was used, since the higher the scan frequency, the wavier the CODSs. However, for the CODSs at the third and fourth excitation frequencies, their qualities were consistently high for different scan frequencies. It is recommended that a relatively low scan frequency be used in order to guarantee CODSs of high qualities, and a relatively high scan frequency be used when only ODSs are to be measured. In addition,

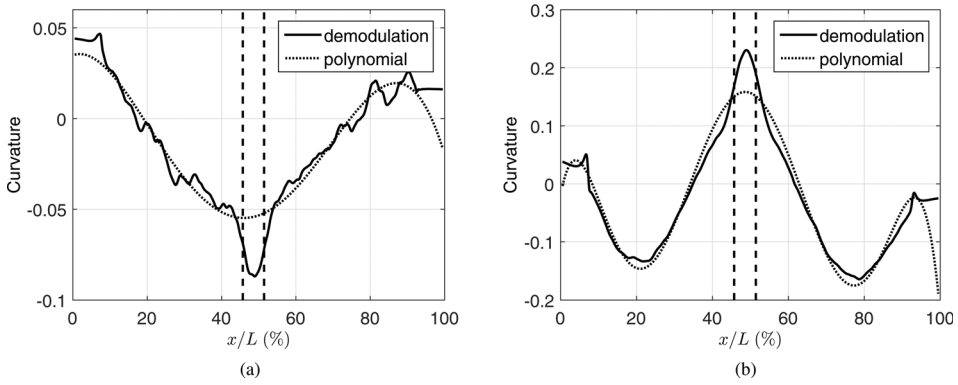

Fig. 20 Comparisons between CODSs from the demodulation and polynomial methods when the beam was excited at frequencies of (*a*) 200 Hz and (*b*) 850 Hz. Locations of damage ends are indicated by two vertical dashed lines.

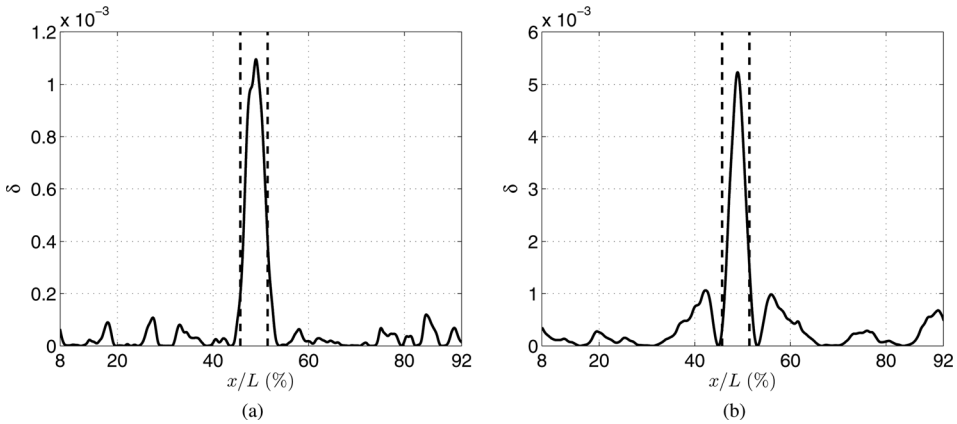

Fig. 21 CDIs at excitation frequencies of (*a*) 200 Hz and (*b*) 850 Hz. Locations of damage ends are indicated by two vertical dashed lines.

there were retortions near the locations 7% and 93% on the scan line possibly due to changes of the scan direction of the laser spot during measurements.

3.1.2 ODSs and CODSs From the Polynomial Method. ODSs and CODSs of the beam at the same excitation and scan frequencies as those in Sec. 3.1.1 were obtained by the polynomial method with a sampling frequency of 32,000 Hz, as shown in Figs. 11 and 12, respectively. Unlike the demodulation method, scan frequencies did not have significant effects on both the ODSs and CODSs in the polynomial method. It could be seen that the damage did not cause any abrupt local abnormalities to the CODSs in the neighborhood of the damage as if there had been no damage in the beam. Hence, the CODSs could be considered to be those of an associated undamaged beam for damage identification if orders in the polynomial method were properly determined. Proper values of m in the polynomial method can be determined based on the guideline proposed in Sec. 2.2.2. Convergence indices con(m) with m up to 14 for the ODSs at the four excitation frequencies are shown in Fig. 13; m for the ODSs at the first through fourth excitation frequencies were determined to be five, seven, eight, and nine, respectively, and resulting ODSs and CODSs are shown in Figs. 11 and 12, respectively.

3.2 Effects of the Sampling Frequency of the CSLDV System. ODSs of the beam at the excitation frequencies were obtained by the demodulation and polynomial methods with a scan frequency of 0.2 Hz and different sampling frequencies of 1600 Hz, 3200 Hz, 16,000 Hz, and 32,000 Hz, as shown in Figs. 14 and 15, respectively. Note that ODSs at 1193 Hz from the two methods with a sampling frequency of 1600 Hz were not included to avoid aliasing. It could be observed that the ODSs from the two methods at each excitation frequency, though measured with different sampling frequencies, agreed well with one another.

CODSs associated with the ODSs from the demodulation and polynomial methods are shown in Figs. 16 and 17, respectively. Similar to Sec. 3.1.1, measurement noise in the ODSs from the demodulation method was reduced by applying the numerical smoothing method. It could be seen that qualities of the CODSs from the demodulation method were not affected by the sampling frequency of the CSLDV system and local abrupt abnormalities in the form of a prominent peak existed in the damage region. Similar to the CODSs from the demodulation method, the sampling frequency did not have significant effects on CODSs from the polynomial method either.

3.3 Damage Identification Results. Comparisons between the CODSs of the damaged beam from the demodulation and polynomial methods at the four excitation frequencies with a scan frequency of 0.2 Hz and a sampling frequency of 32,000 Hz are shown in Fig. 18. It could be seen that there were abrupt local abnormalities in the CODSs from the demodulation method in the neighborhood of the damage, as opposed to the CODSs from the polynomial method. CDIs in Eq. (17) are shown in Fig. 19; note that CDIs in intervals from 0% to 8% and from 92% to 100% are not shown, and there were discrepancies between CODSs associated with ODSs from the demodulation and polynomial methods, which would occur even when no damage existed in the intervals, similar to the numerical case shown in Fig. 1(*d*). In the CDIs shown in Fig. 19, prominent peaks could be clearly identified in the neighborhood of the damage, and smaller peaks that were caused by measurement noise could also be identified. One could identify the damage and its region along the scan line on the beam based on the CDIs at the four excitation frequencies.

3.4 Damage Identification Results at Arbitrary Excitation Frequencies. In order to show robustness of the proposed methodology, the beam was excited at 200 Hz and 850 Hz that were arbitrarily selected and not close to any of its natural frequencies, and ODSs were obtained by the two methods. CODSs associated with the ODSs are shown in Fig. 20, and it can be seen that their amplitudes were much smaller than those at the first four natural frequencies of the beam (Fig. 18). A possible consequence for a CODS with a small amplitude is that effects of damage are fuzzed in the CODS by those of measurement noise and damage becomes unidentifiable. In order to alleviate adverse effects of measurement noise, one can improve an experimental setup by increasing the level of excitation and/or lowering the scan frequency of the CSLDV system. In this experiment, effects of the damage on the CODSs from the two methods could be seen by comparing them, due to the fact that the beam was well excited by the shaker and the scan frequency of the system was sufficiently low. Note that m in the polynomial method for the ODSs at 200 Hz and 850 Hz were determined to be six and eight, respectively, based on the guideline in Sec. 2.2.2. The damage and its region could be clearly identified in neighborhoods of prominent peaks in the CDIs at the two excitation frequencies (Fig. 21). The reason was that an ODS at an excitation frequency that is not a natural frequency can be considered as a sum of mode shapes with their participation factors determined by the excitation frequency and the damage and its region could be identified using mode shapes or ODSs at natural frequencies (Fig. 19). Hence the proposed damage identification methodology is applicable to an ODS at an arbitrary excitation frequency. The proposed methodology can be used to identify small-sized damage, such as a crack, if an experiment is well set up: the level of excitation is sufficiently high and the scan frequency is sufficiently low. Boundary conditions of the beam do not affect effectiveness of the proposed methodology, since its main idea is that damage can result in local abrupt abnormalities

in a CODS in the damage region and one can identify the damage by comparing the CODSs from the two methods and locating the abrupt abnormalities. For a nonlinear beam excited at a given frequency, the shape of its ODS can depend on the amplitude of excitation. Effects of damage on the beam can still exist in an ODS and be manifested in the associated CODS in the damage region; hence the damage can be identified using the proposed methodology.

4 Conclusion

A CSLDV system is first used to identify damage in beams without use of any baseline information of associated undamaged beams. A CDI that uses the difference between in-phase components of CODSs from the demodulation and polynomial methods is proposed to identify damage. The demodulation method provides rapid and spatially dense ODSs of beams, and the polynomial method provides ODSs that can be considered as those of associated undamaged beams if the beams are geometrically smooth and made of materials that have no stiffness discontinuities. Amplitudes of in-phase and quadrature components of an ODS can be maximized and minimized, respectively, by optimizing phase variables introduced in the two methods for damage identification purposes. Effects of scan and sampling frequencies of the CSLDV system on ODSs and CODSs obtained by the two methods are investigated. While the scan frequency does not affect qualities of ODSs from the demodulation method, it affects those of some CODSs. A low scan frequency is recommended to obtain CODSs of high qualities. The scan frequency does not affect qualities of ODSs and CODSs from the polynomial method, but the order in the polynomial method affects qualities of ODSs and CODSs. As the order increases, an ODS converges while the associated CODS does not. To obtain physically correct CODSs for damage identification, a convergence index and a criterion are proposed to determine a proper order in the polynomial method. The sampling frequency does not affect qualities of ODSs and CODSs obtained by the two methods. The proposed damage identification methodology was experimentally applied to a damaged beam with a machined thickness reduction along the length of the beam. The damage and its region were successfully identified in neighborhoods of prominent peaks of CDIs at different excitation frequencies including those that were not close to natural frequencies of the beam. For an ODS at an excitation frequency that is not a natural frequency, one can increase the level of excitation and/or lower the scan frequency of the CSLDV to alleviate adverse effects of measurement noise.

Acknowledgment

The authors are grateful for the financial support from the National Science Foundation under Grant Nos. CMMI-1229532 and CMMI-1335024.

Appendix: Calculation of $\mathbf{T}_{m+1}$

When $m=2$, $\sum_{n=0}^{m} V_{In}\cos^n(\Omega t+\beta)\cos\omega t$ in Eq. (12) can be expanded as

$$\begin{aligned}
&\sum_{n=0}^{2} V_{In}\cos^n(\Omega t+\beta)\cos\omega t\\
&= V_{I0}\cos^0(\Omega t+\beta)\cos\omega t + V_{I1}\cos^1(\Omega t+\beta)\cos\omega t + V_{I2}\cos^0(\Omega t+\beta)\cos\omega t\\
&= V_{I0}\cos\omega t + \frac{V_{I1}}{2}[\cos(\omega t-\Omega t-\beta)+\cos(\omega t+\Omega t+\beta)] + \frac{V_{I2}}{2}\cos(\Omega t+\beta)[\cos(\omega t-\Omega t-\beta)+\cos(\omega t+\Omega t+\beta)]\\
&= \left(V_{I0}+\frac{V_{I2}}{2}\right)\cos\omega t + \frac{V_{I1}}{2}[\cos(\omega t-\Omega t-\beta)+\cos(\omega t+\Omega t+\beta)] + \frac{V_{I2}}{4}[\cos(\omega t-2\Omega t-2\beta)+\cos(\omega t+2\Omega t+2\beta)]\\
&= A_{I0}\cos\omega t + A_{I1}[\cos(\omega t-\Omega t-\beta)+\cos(\omega t+\Omega t+\beta)] + A_{I2}[\cos(\omega t-2\Omega t-2\beta)+\cos(\omega t+2\Omega t+2\beta)] \qquad \text{(A1)}
\end{aligned}$$

and a similar expansion of $\sum_{n=0}^{m} V_{Qn}\cos^n(\Omega t+\beta)\sin\omega t$ in Eq. (12) yields

$$\begin{aligned}
&\sum_{n=0}^{2} V_{Qn}\cos^n(\Omega t+\beta)\sin\omega t\\
&= \left(V_{Q0}+\frac{V_{Q2}}{2}\right)\sin\omega t + \frac{V_{Q1}}{2}[\sin(\omega t-\Omega t-\beta)+\sin(\omega t+\Omega t+\beta)] + \frac{V_{Q2}}{4}[\sin(\omega t-2\Omega t-2\beta)+\sin(\omega t+2\Omega t+2\beta)]\\
&= A_{Q0}\sin\omega t + A_{Q1}[\sin(\omega t-\Omega t-\beta)+\sin(\omega t+\Omega t+\beta)] + A_{Q2}[\sin(\omega t-2\Omega t-2\beta)+\sin(\omega t+2\Omega t+2\beta)] \qquad \text{(A2)}
\end{aligned}$$

A matrix $\mathbf{U}_3$ that relates V_{In} to A_{In} in Eq. (A1) and V_{Qn} to A_{Qn} in Eq. (A2) can be defined as

$$\begin{cases} \mathbf{A}_I = \mathbf{U}_3\mathbf{V}_I \\ \mathbf{A}_Q = \mathbf{U}_3\mathbf{V}_Q \end{cases} \qquad \text{(A3)}$$

where

$$\mathbf{U}_3 = \begin{bmatrix} 1 & 0 & \frac{1}{2} \\ 0 & \frac{1}{2} & 0 \\ 0 & 0 & \frac{1}{4} \end{bmatrix} \qquad \text{(A4)}$$

and $\mathbf{T}_3$ that relates A_{In} to V_{In} in Eq. (A1) and A_{Qn} to V_{Qn} in Eq. (A2) is

$$\mathbf{T}_3 = \mathbf{U}_3^{-1} = \begin{bmatrix} 1 & 0 & -2 \\ 0 & 2 & 0 \\ 0 & 0 & 4 \end{bmatrix} \qquad \text{(A5)}$$

One can calculate $\mathbf{T}_{m+1}$ in a way similar to that for $\mathbf{T}_3$. When $m=15$, one has [23]

$$\mathbf{T}_{16} = \begin{bmatrix}
1 & 0 & -2 & 0 & 2 & 0 & -2 & 0 & 2 & 0 & -2 & 0 & 2 & 0 & -2 & 0 \\
0 & 2 & 0 & -6 & 0 & 10 & 0 & -14 & 0 & 18 & 0 & -22 & 0 & 26 & 0 & -30 \\
0 & 0 & 4 & 0 & -16 & 0 & 36 & 0 & -64 & 0 & 100 & 0 & -144 & 0 & 196 & 0 \\
0 & 0 & 0 & 8 & 0 & -40 & 0 & 112 & 0 & -240 & 0 & 440 & 0 & -728 & 0 & 1120 \\
0 & 0 & 0 & 0 & 16 & 0 & -96 & 0 & 320 & 0 & -800 & 0 & 1680 & 0 & -3136 & 0 \\
0 & 0 & 0 & 0 & 0 & 32 & 0 & -224 & 0 & 864 & 0 & -2464 & 0 & 5824 & 0 & -12096 \\
0 & 0 & 0 & 0 & 0 & 0 & 64 & 0 & -512 & 0 & 2240 & 0 & -7168 & 0 & 18816 & 0 \\
0 & 0 & 0 & 0 & 0 & 0 & 0 & 128 & 0 & -1152 & 0 & 5632 & 0 & -19968 & 0 & 57600 \\
0 & 0 & 0 & 0 & 0 & 0 & 0 & 0 & 256 & 0 & -2560 & 0 & 13824 & 0 & -53760 & 0 \\
0 & 0 & 0 & 0 & 0 & 0 & 0 & 0 & 0 & 512 & 0 & -5632 & 0 & 33280 & 0 & -140800 \\
0 & 0 & 0 & 0 & 0 & 0 & 0 & 0 & 0 & 0 & 1024 & 0 & -12288 & 0 & 78848 & 0 \\
0 & 0 & 0 & 0 & 0 & 0 & 0 & 0 & 0 & 0 & 0 & 2048 & 0 & -26624 & 0 & 184320 \\
0 & 0 & 0 & 0 & 0 & 0 & 0 & 0 & 0 & 0 & 0 & 0 & 4096 & 0 & -57344 & 0 \\
0 & 0 & 0 & 0 & 0 & 0 & 0 & 0 & 0 & 0 & 0 & 0 & 0 & 8192 & 0 & -122880 \\
0 & 0 & 0 & 0 & 0 & 0 & 0 & 0 & 0 & 0 & 0 & 0 & 0 & 0 & 16384 & 0 \\
0 & 0 & 0 & 0 & 0 & 0 & 0 & 0 & 0 & 0 & 0 & 0 & 0 & 0 & 0 & 32768
\end{bmatrix} \tag{A6}$$

Note that $\mathbf{T}_{m+1}$ with m up to 15 can be formed by extracting entries of the first $m+1$ rows and first $m+1$ columns of $\mathbf{T}_{16}$ above.

References

[1] Doebling, S. W., Farrar, C. R., and Prime, M. B., 1998, "A Summary Review of Vibration-Based Damage Identification Methods," Shock Vib. Dig., **30**(2), pp. 91–105.

[2] Xu, G. Y., Zhu, W. D., and Emory, B. H., 2007, "Experimental and Numerical Investigation of Structural Damage Detection Using Changes in Natural Frequencies," ASME J. Vib. Acoust., **129**(6), pp. 686–700.

[3] He, K., and Zhu, W. D., 2010, "Detection of Damage and Loosening of Bolted Connections in Structures Using Changes in Natural Frequencies," ASNT Mater. Eval., **68**(6), pp. 721–732.

[4] Zhu, W. D., and He, K., 2013, "Detection of Damage in Space Frame Structures With L-Shaped Beams and Bolted Joints Using Changes in Natural Frequencies," ASME J. Vib. Acoust., **135**(5), p. 051001.

[5] He, K., and Zhu, W. D., 2014, "Detecting Loosening of Bolted Connections in a Pipeline Using Changes in Natural Frequencies," ASME J. Vib. Acoust., **136**(3), p. 034503.

[6] Pandey, A. K., Biswas, M., and Samman, M. M., 1991, "Damage Detection From Changes in Curvature Mode Shapes," J. Sound Vib., **145**(2), pp. 321–332.

[7] Ratcliffe, C. P., 2000, "A Frequency and Curvature Based Experimental Method for Locating Damage in Structures," ASME J. Vib. Acoust., **122**(3), pp. 324–329.

[8] Yoon, M. K., Heider, D., Gillespie, J. W., Jr., Ratcliffe, C. P., and Crane, R. M., 2009, "Local Damage Detection With the Global Fitting Method Using Mode Shape Data in Notched Beams," J. Nondestr. Eval., **28**(2), pp. 63–74.

[9] Xu, Y. F., Zhu, W. D., Liu, J., and Shao, Y. M., 2014, "Identification of Embedded Horizontal Cracks in Beams Using Measured Mode Shapes," J. Sound Vib., **333**(23), pp. 6273–6294.

[10] Xu, W., Zhu, W. D., Smith, S. A., and Cao, M. S., 2016, "Structural Damage Detection Using Slopes of Longitudinal Mode Shapes," ASME J. Vib. Acoust., **138**(3), p. 034501.

[11] Rothberg, S., Baker, J., and Halliwell, N. A., 1989, "Laser Vibrometry: Pseudo-Vibrations," J. Sound Vib., **135**(3), pp. 516–522.

[12] Sriram, P., Hanagud, S., Craig, J., and Komerath, N., 1990, "Scanning Laser Doppler Technique for Velocity Profile Sensing on a Moving Surface," Appl. Opt., **29**(16), pp. 2409–2417.

[13] Sriram, P., Hanagud, S., and Craig, J., 1992, "Mode Shape Measurement Using a Scanning Laser Doppler Vibrometer," Int. J. Anal. Exp. Modal Anal., **7**(3), pp. 169–178.

[14] Stanbridge, A., and Ewins, D., 1996, "Using a Continuously-Scanning Laser Doppler Vibrometer for Modal Testing," 14th International Modal Analysis Conference (IMAC), Dearborn, MI, Feb. 12–15, pp. 816–822.

[15] Stanbridge, A., and Ewins, D., 1999, "Modal Testing Using a Scanning Laser Doppler Vibrometer," Mech. Syst. Signal Process., **13**(2), pp. 255–270.

[16] Stanbridge, A., Ewins, D., and Khan, A., 2000, "Modal Testing Using Impact Excitation and a Scanning LDV," Shock Vib., **7**(2), pp. 91–100.

[17] Di Maio, D., and Ewins, D., 2011, "Continuous Scan, a Method for Performing Modal Testing Using Meaningful Measurement Parameters; Part I," Mech. Syst. Signal Process., **25**(8), pp. 3027–3042.

[18] Allen, M. S., and Sracic, M. W., 2010, "A New Method for Processing Impact Excited Continuous-Scan Laser Doppler Vibrometer Measurements," Mech. Syst. Signal Process., **24**(3), pp. 721–735.

[19] Yang, S., and Allen, M. S., 2014, "Lifting Approach to Simplify Output-Only Continuous-Scan Laser Vibrometry," Mech. Syst. Signal Process., **45**(2), pp. 267–282.

[20] Yang, S., and Allen, M. S., 2014, "Harmonic Transfer Function to Measure Translational and Rotational Velocities With Continuous-Scan Laser Doppler Vibrometry," ASME J. Vib. Acoust., **136**(2), p. 021025.

[21] Khan, A., Stanbridge, A. B., and Ewins, D. J., 1999, "Detecting Damage in Vibrating Structures With a Scanning LDV," Opt. Lasers Eng., **32**(6), pp. 583–592.

[22] Cox, I., and Gaudard, M., 2013, *Discovering Partial Least Squares With JMP*, SAS Institute, Cary, NC.

[23] Martarelli, M., 2001, "Exploiting the Laser Scanning Facility for Vibration Measurements," Ph.D. thesis, University of London, London, UK.